

Quasinormal modes, shadow and thermodynamics of black holes coupled with nonlinear electrodynamics and cloud of strings

Dharm Veer Singh^{a,1,†} Aradhya Shukla,^{1,‡} and Sudhaker Upadhyay^{da2,3,¶}

¹*Department Physics, GLA University, Mathura 281406 Uttar Pradesh*

²*Department of Physics, K.L.S. College, Magadh University, Nawada, Bihar 805110, India*

³*School of Physics, Damghan University, P.O. Box 3671641167,
Damghan, Iran*

We construct an exact black hole solution for the Einstein gravity coupled with the nonlinear electrodynamics (which corresponds to the Maxwell electrodynamics in the weak field limit) in the presence of a cloud of strings as the source. We study the thermodynamical properties of the black hole solutions and derive the corrected first-law of thermodynamics. The presence of a cloud of strings does not affect the stability of the present black hole. However, a second-order phase transition exists for this system at a critical horizon radius. Furthermore, we study the quasinormal modes and their shadow radius. In addition, we find that, upon variation, the parameters of the theory show different aspects of the optical characteristics of the black hole solutions.

Keywords: Quasinormal modes; Black holes shadow; Black holes thermodynamics.

I. INTRODUCTION

One of the important aspects of general relativity is to find solutions to Einstein's field equation. The metric tensor in arbitrarily chosen spacetimes may lead to an unphysical stress-tensor. Therefore, obtaining a meaningful solution to Einstein's field equation is a cumbersome job [1]. The well-known vacuum (without matter) solution and with matter solution of Einstein's field equation is the Schwarzschild black hole and Reissner-Nordström black hole, respectively. These spherically symmetric solutions have a central singularity which is separated by a boundary known as the event horizon. On the other hand, non-singular solutions of Einstein's field equations are known as regular black holes. Indeed, one can have black hole metrics without a physical singularity. Bardeen was the first to realize the idea of a central matter core and to propose a regular black hole solution with horizons (but without a singularity) [2]. The Bardeen regular black hole is a spherically symmetric solution that violates the strong energy condition. Furthermore, other spherically symmetric regular solutions were proposed [3–5]. There has been tremendous development in the investigations of regular black hole solutions and their properties [6–9]. Recently, it is observed that regular black hole solutions with spherical symmetry violate the weak energy condition [10].

It has been observed that the linearity of the real electromagnetic field breaks at high energies due to interactions with other physical fields. In such circumstances, the most suitable alternative is nonlinear electrodynamics as a simplified phenomenological description of this interaction. The properties of the nonlinear electrodynamics can be lucid from the perspective of gravity since strong vector fields are dominant at the center of black holes. The behavior of charged particles around black holes may be described by nonlinear electrodynamics. Hence, it is crucial to emphasize the gravitational field coupled to nonlinear electrodynamics. Born and Infeld were the first to propose nonlinear electrodynamics with the motivation to have a finite self-energy of the point charge [11]. Moreover, a lot of progress have been made in various contexts [12–16]. Nonlinear electrodynamics also gets relevance as a generalized Born-Infeld action appears naturally from the effective string action [17, 18].

Letelier proposed a model analogous to pressure-less perfect fluid known as cloud of strings (CS) [19]. From this perspective, a generalized Schwarzschild black hole solution is obtained in the background of a spherically symmetric cloud of strings [20, 21]. However, the energy-momentum tensor of the string manifests a non-null pressure, which therefore leads to astrophysical and cosmological implications. Further studies of a cloud of strings in the general relativity and alternative theories of gravity are reported in Refs. [22–27]. Since strings are supposed to be fundamental constituents of the universe rather than point-like particles. This derives us to study the black hole solutions in presence of CS. More precisely, we provide an exact solution for the Einstein gravity coupled to nonlinear electrodynamics in presence of a cloud of strings. We also discuss its thermodynamics, stability and phase transition.

^aVisiting Associate, IUCAA Pune, Maharashtra 411007, India

^dCorresponding author

[†] veerdsingh@gmail.com; dharm.singh@associates.iucaa.in

[‡] ashukla038@gmail.com

[¶] sudhakerupadhyay@gmail.com; sudhaker@associates.iucaa.in

Let us briefly introduce CS as matter source. The CS is governed by the Nambu-Goto action, which takes the form

$$S_{\text{NG}} = \int_{\Sigma} m(-\gamma)^{-1/2} d\lambda^0 d\lambda^1 = \int_{\Sigma} m \left(-\frac{1}{2} \Sigma^{\mu\nu} \Sigma_{\mu\nu} \right)^{1/2} d\lambda^0 d\lambda^1, \quad (1)$$

where constant m characterizes each string, (λ^0, λ^1) are local coordinates of the string being timelike and spacelike in nature, respectively [28]. Here, γ refers to the determinant of an induced metric $\gamma_{ab} := g_{\mu\nu} \frac{\partial x^\mu}{\partial \lambda^a} \frac{\partial x^\nu}{\partial \lambda^b}$ on the strings world sheet. The bivector related to the string world sheet Σ is written by

$$\Sigma^{\mu\nu} = \epsilon^{ab} \frac{\partial x^\mu}{\partial \lambda^a} \frac{\partial x^\nu}{\partial \lambda^b}, \quad (2)$$

where second rank Levi-Civita tensor ϵ^{ab} (anti-symmetric in a and b) takes following non-zero values: $\epsilon^{01} = -\epsilon^{10} = 1$.

Using definition, $T^{\mu\nu} = 2 \frac{\partial}{\partial g_{\mu\nu}} m \left(-\frac{1}{2} \Sigma^{\mu\nu} \Sigma_{\mu\nu} \right)^{1/2}$, we obtain single string energy-momentum tensor as $T^{\mu\nu} = \frac{m \Sigma^{\mu\rho} \Sigma_{\rho}^{\nu}}{\sqrt{-\gamma}}$. Since the CS is characterized by a proper density ρ rather than a single mass, therefore, the energy-momentum tensor for CS is given by

$$T^{\mu\nu} = \frac{\rho \Sigma^{\mu\rho} \Sigma_{\rho}^{\nu}}{\sqrt{-\gamma}}. \quad (3)$$

Here, $\rho (\gamma)^{-1/2}$ denotes a gauge-invariant density.

The only surviving component of the bivector Σ regarding spherically symmetric solution is $\Sigma^{tr} = -\Sigma^{rt}$. Thus, conservation law leads to

$$T_t^t = T_r^r = \frac{a}{r^2}, \quad (4)$$

for some real constant a , which is related to the global monopole charge[29].

The proper solutions of the perturbation equations of a black hole belonging to certain complex characteristic frequencies (which satisfy the boundary conditions) are described by quasinormal modes (QNMs) [30]. A close connection exists between QNMs and the shadow radius of a black hole [31]. The QNMs are determined entirely by the dynamics of black holes. At the same time, the shadow radius belongs to optical properties, such a connection justifies the relation between dynamics and optical properties of black holes [32, 33]. Recently, the shadow of the 5D AdS Reissner-Nordström black hole is studied in Ref. [34].

The paper is structured as follows. In section II, we consider an action describing Einstein's gravity with nonlinear electrodynamics in the presence of CS. We obtain an exact black hole solution with coordinate singularity for this model in section III. Here, we discuss the energy conditions for this black hole solution. Thermodynamical behavior of this black hole is presented in section IV. We see that the black hole follows a modified first-law of thermodynamics. We study the photon radius including shadow radius in section V. Within the section, we consider a photon moving in a circular orbit. The photon radius is obtained numerically. The section VI is devoted to the study of the connection between shadow radius and QNMs. We conclude the results and their importance in the last section.

II. GRAVITY COUPLED WITH NONLINEAR ELECTRODYNAMICS AND CLOUD OF STRINGS

Now, the action describing Einstein's gravity coupled to nonlinear electrodynamics and surrounded by a CS in 4 dimensions is given by

$$S = \frac{1}{2} \int_{\mathcal{M}} d^4x \sqrt{-g} [R + \mathcal{L}(\mathcal{F})] + S_{\text{NG}}, \quad (5)$$

the Lagrangian $\mathcal{L}(\mathcal{F})$ describes nonlinear electrodynamics with invariant $\mathcal{F} = \frac{1}{4} F_{\mu\nu} F^{\mu\nu}$, where $F_{\mu\nu} = \nabla_\mu A_\nu - \nabla_\nu A_\mu$ is the electromagnetic field strength tensor for the gauge potential A_ν .

The equations of motion for the action are given by [35]

$$G_{\mu\nu} \equiv R_{\mu\nu} - \frac{1}{2} g_{\mu\nu} R = \mathcal{T}_{\mu\nu} + T_{\mu\nu}, \quad (6)$$

$$\nabla_\mu \left(\frac{\partial \mathcal{L}(\mathcal{F})}{\partial \mathcal{F}} F_{\mu\nu} \right) = 0 \quad \text{and} \quad \nabla_\mu (*F_{\mu\nu}) = 0. \quad (7)$$

where $G_{\mu\nu}$ is the Einstein tensor and $\mathcal{T}_{\mu\nu} \equiv 2 \left[\frac{\partial \mathcal{L}}{\partial \mathcal{F}} F_{\mu\rho} F_{\nu}^{\rho} - g_{\mu\nu} \mathcal{L} \right]$ is energy-momentum tensor related to the electromagnetic tensor. The explicit form of Lagrangian density of the nonlinear electrodynamics is considered as [36]

$$\mathcal{L}(\mathcal{F}) = \mathcal{F} e^{-\frac{k}{q}(2q^2 \mathcal{F})^{\frac{1}{4}}}, \quad \text{with} \quad k = \frac{q^2}{2M}. \quad (8)$$

Here, q corresponds to the nonlinear charge of a self-gravitating magnetic field and M is the mass parameter, later which is related to the mass of the black hole. The Lagrangian $\mathcal{L}(\mathcal{F})$ is the function of \mathcal{F} , where the Lagrangian $\partial \mathcal{L} / \partial \mathcal{F} \rightarrow \infty$ as $\mathcal{F} \rightarrow \infty$ and $\partial \mathcal{L} / \partial \mathcal{F} \rightarrow 1$ as $\mathcal{F} \rightarrow 0$. In weak field limit ($\mathcal{F} \ll 1$), the \mathcal{L} identifies to the Maxwell electrodynamics. Nonetheless, under the strong field limit, \mathcal{L} vanishes.

We consider the following *ansatz* for the Maxwell field [37, 38]:

$$F_{\mu\nu} = 2\delta_{[\mu}^{\theta_1} \delta_{\nu]}^{\theta_2} q \sin \theta. \quad (9)$$

with \mathcal{F} as

$$\mathcal{F} = \frac{q^2}{2r^4}. \quad (10)$$

The energy-momentum tensor, in this case, is calculated by

$$\mathcal{T}_t^t = \mathcal{T}_r^r = \frac{2Mk e^{-\frac{q^2}{2Mr}}}{r^4}, \quad (11)$$

which satisfies the equations of motion in the case of nonlinear electrodynamics.

III. REGULAR BLACK HOLE SOLUTIONS WITH CLOUD OF STRINGS

In this section, the main motivation is to get a static spherically symmetric solution of the equation of motion (6) with a CS and nonlinear electrodynamics as source and investigate its properties. In order to achieve the goal, let us begin by writing spherically symmetric static metric of the form:

$$ds^2 = -f(r)dt^2 + \frac{1}{f(r)}dr^2 + r^2 d\Omega^2, \quad (12)$$

with

$$f(r) = 1 - \frac{2m(r)}{r}, \quad (13)$$

where $d\Omega^2 = d\theta^2 + \sin^2 \theta d\phi^2$ is the metric on $2D$ sphere. Using Eq. (6) with the metric element (13) leads to the Einstein field equations to have the following form:

$$\frac{d}{dr}m(r) = \frac{q^2}{2r^2} e^{-k/r} + \frac{a}{2}. \quad (14)$$

Integrating the above expression (14), we have the explicit form of single string mass

$$m(r) = M e^{-k/r} + \frac{a}{2}r + C_1, \quad (15)$$

where C_1 is constant, then $C_1 = \lim_{r \rightarrow \infty} m(r) - ar = M$ and substituting the $m(r)$ into $f(r)$, the black hole solution (12) becomes

$$ds^2 = - \left[1 - \frac{2M}{r} e^{-k/r} - a \right] dt^2 + \frac{1}{\left[1 - \frac{2M}{r} e^{-k/r} - a \right]} dr^2 + r^2 d\Omega^2. \quad (16)$$

This is an exact black hole solution in the presence of nonlinear source $e^{-k/r}$ and CS parameter a . This black hole is characterized by the parameters like M , k and a . The presence of such a nonlinear source and CS parameter ensure deviation from Schwarzschild black hole. In the limit $k = 0$, the resulting solution reduces to Letelier solution [21]. However, this coincides to Schwarzschild black hole solution for $k = 0$ and $a = 0$. The solution behaves as the

Reissner-Nordström black hole for the case of $r \gg k$. For $a = 0$ and $k < 0$, $m(r)$ increases exponentially for small r . On the other hand, when $k > 0$, $m(r)$ has the following properties:

$$\lim_{r \rightarrow 0^+} e^{-k/r} + a = a, \quad \lim_{r \rightarrow 0^-} e^{-k/r} + a = +\infty. \quad (17)$$

The function is discontinuous at $r = 0$. For $r \gg k$, the obtained solution behaves as a Reissner-Nordström black hole with CS parameter a as

$$f(r) = 1 - \frac{2M}{r} + \frac{q^2}{r^2} - a + \mathcal{O}\left(\frac{k^2}{r^2}\right). \quad (18)$$

The charge q and mass M are related by the relation $q^2 = 2Mk$ as mentioned in (8). It is not cumbersome to estimate the numerical range of M , a and k for the black hole solution (16). This black hole has two horizons, the event horizon (r_+) and the Cauchy horizon (r_-). These horizons in terms of the Lambert W function are given by

$$r_{\pm} = -\frac{k}{W\left(-\frac{(1-a)k}{2M}\right)} \quad \Rightarrow \quad r_{\pm} = \frac{2M}{(1-a)} e^{W\left(-\frac{(1-a)k}{2M}\right)}. \quad (19)$$

The Lambert W function has two branches W_0 and W_{-1} and provides two possibilities,

$$\begin{aligned} W_0\left(-\frac{(1-a)k}{2M}\right) < 0 & \quad \Rightarrow \quad k \in \left(0, \frac{2M}{(1-a)q}\right], \\ W_{-1}\left(-\frac{(1-a)k}{2M}\right) < 0, & \quad \Rightarrow \quad k \in \left[-\frac{2M}{(1-a)q}, 0\right). \end{aligned} \quad (20)$$

The value of k lies in this interval as we have well defined coordinate location for a horizon when taking the $(-(1-a)k/M)$ branch of the Lambert function. The range W_{-1} branch is entirely $-ve$ and only return output occurs when $[-M/(1-a)q, 0)$. This means that all the possible solutions will correspond to $r_+ > 0$. The inner and event horizons are located at, respectively,

$$r_- = \frac{2M}{(1-a)} e^{W_{-1}\left(-\frac{(1-a)k}{2M}\right)}, \quad \text{and} \quad r_+ = \frac{2M}{(1-a)} e^{W_0\left(-\frac{(1-a)k}{2M}\right)}. \quad (21)$$

Only for $k = 2M/(1-a)q$, the inner and event horizon coincides and we have an extremal black hole. Moreover, for $k > 2M/(1-a)q$, the Lambert W function is undefined. In order to study the behavior of $f(r)$ as a function of the different parameters, we plot figure 1. However, the numerical analysis of the horizon is tabulated in TABLE I.

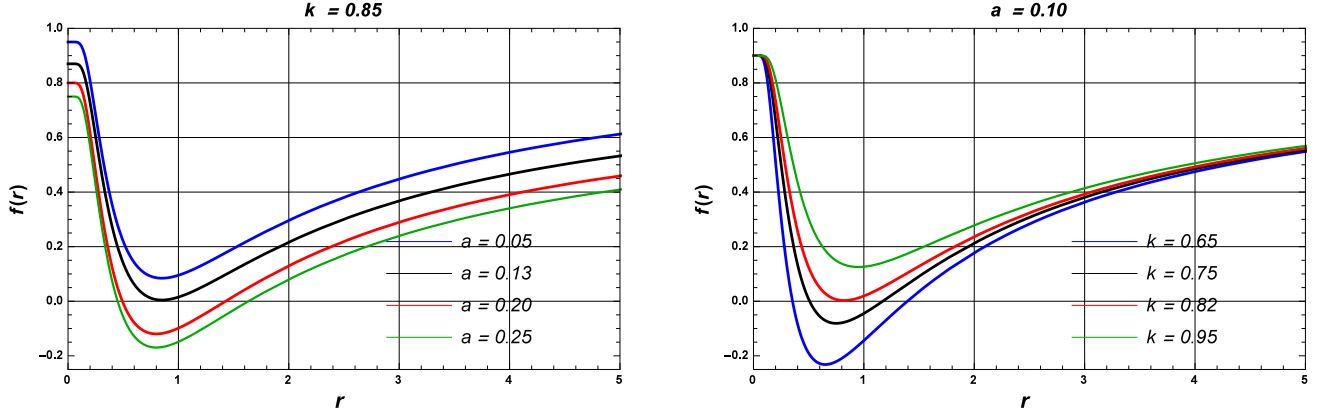


FIG. 1. The plot of metric function $f(r)$ versus horizon radius r for different value of CS parameter a (in the left plot) and deviation parameter k (in the right plot).

From the figure 1, we can see that the metric function of the black hole increases with increasing CS parameter (a) and the metric of the black hole decreases with increasing deviation parameter (k). It is worthwhile to mention that the behavior of the CS parameter is opposite to the deviation parameter. The numerical analysis suggests that the inner horizon decreases with increasing a and decreasing k . However, the outer horizon increases with increasing a and decreasing k .

a	$k = 0.85$			$a = 0.10$			
	r_-	r_+	δ	k	r_-	r_+	δ
0.13	0.875	0.875	0	0.65	0.357	1.39	1.037
0.20	0.587	1.313	0.726	0.75	0.518	1.175	0.657
0.25	0.518	1.509	0.991	0.813	0.904	0.904	0

TABLE I. Radius of inner and outer horizons and $\delta = r_+ - r_-$ for different values of charge q .

IV. THERMODYNAMICS

Now, we analyze the thermodynamical quantities associated with the black hole solution (16) which is characterized by parameters M , k and a . The black hole mass M can be obtained by setting metric function $f(r) = 0$ at horizon radius r_+ . This gives

$$M_+ = \frac{(1-a)}{2} r_+ e^{k/r_+}. \quad (22)$$

This expression exactly coincides with the mass of the regular black hole for $a = 0$, however, this matches with the mass of the Schwarzschild black hole for the vanishing deviation parameter and CS parameter.

The Hawking temperature (T_+) evaluated at the horizon is directly related to the surface gravity κ given by [39, 40]

$$\kappa = \left(-\frac{1}{2} \nabla_\mu \xi_\nu \nabla^\mu \xi^\nu \right)^{1/2} = \frac{1}{2} f'(r_+), \quad (23)$$

and $\xi^\mu = \partial/\partial t$ is a Killing vector. This form of Hawking temperature can also be derived from the tunneling method [41]. Corresponding to black hole solution (16), the Hawking temperature is calculated by

$$T_+ = \frac{(1-a)}{4\pi r_+} \left[1 - \frac{k}{r_+} \right]. \quad (24)$$

From the above expression, it is obvious that, for $k = 0$ and $a = 0$, the Hawking temperature reduces to $T_+ = 1/4\pi r_+$ which is exactly identified with the case of Schwarzschild black holes.

Next, we would like to study the entropy of our black hole solution. In general, the explicit form of the entropy S_+ can be deduced from the first-law of thermodynamics [42, 43]

$$dM = T_+ dS. \quad (25)$$

In fact, this leads to

$$S_+ = \int \frac{1}{T_+} \frac{\partial M}{\partial r_+} dr_+. \quad (26)$$

Plugging the values of Mass (22) and temperature (24) into (26), we obtain the entropy of our black hole as

$$S_+ = \pi \left(r_+ (k + r_+) e^{k/r_+} - k^2 \text{Ei} \left[\frac{k}{r_+} \right] \right), \quad (27)$$

where the last term is characterized by exponential integral. This entropy does not match with the area-law. However, in the absence of k , this expression exactly matches with the entropy of Schwarzschild black hole. From the expression (27), it is obvious that the area-law is no longer valid for non-singular black holes for large value of k . Now, we can also cross-check the expression of Hawking temperature evaluated from the first-law of thermodynamics (25). Here, we have

$$T_+ = \frac{\partial M_+}{\partial S_+} = \frac{(1-a)}{4\pi r_+} \left[1 - \frac{k}{r_+} \right] e^{-k/r_+}. \quad (28)$$

Here, we see that this expression is not in agreement with one calculated by area-law or tunneling method in (24). Since expressions of black hole temperature (24) and (28) are estimated by two different methods. This means that the first-law of thermodynamics (25) is not appropriate for deriving the black hole temperature for regular black holes.

The modified form of first-law for black holes is presented in Refs. [44, 45]. This modification depends on the general structure of the energy-momentum tensor. In fact, the conventional first-law modifies with an additional factor if the black hole mass parameter is included in the energy-momentum tensor. The modified first-law is, therefore, given as [41, 44, 45]

$$\mathcal{J}(M, r_+) dM = T_+ dS, \quad (29)$$

where correction factor $\mathcal{J}(M, r_+)$ is defined in terms of energy density T_0^0 as

$$\mathcal{J}(M, r_+) = 1 + 4\pi \int_{r_+}^{\infty} r_+^2 \frac{\partial T_0^0}{\partial M} dr_+ = e^{-k/r_+}. \quad (30)$$

The correction factor in our case is calculated by

$$\mathcal{J}(M, r_+) = e^{-k/r}. \quad (31)$$

The entropy following the corrected first-law of thermodynamics (29) is derived as

$$S_+ = \pi r_+^2 = \frac{A}{4}. \quad (32)$$

Obviously, this entropy is in the agreement of the area-law and matches exactly with the entropy of black holes.

The thermodynamical stability of black holes can be understood by studying the heat capacity of the black hole and, therefore, this is calculated by [40, 42]

$$C_+ = \frac{\partial M_+}{\partial T_+} = -4\pi r_+^2 e^{k/r_+} \frac{(1-k)}{2k-r_+}. \quad (33)$$

It is interesting to note that the heat capacity obtained in the above equation is independent of a CS parameter. This suggests that the stability/instability of the present black hole is not affected by the presence of CS. We also check a second-order phase transition (Davies point) in the above-obtained solution, where the temperature of the black hole is maximum ($dT_+/dr_+ = 0$). The heat capacity shows two opposite behaviors: one of them is negative in the region $r_+ < r_C$ (critical radius) which justifies the thermodynamic instability of black hole and, for the region $r_+ > r_C$, this is positive which warrants the black hole stability. In fact, the heat capacity is discontinuous at $r_+ = r_C$ and divergence occurs, which conforms the existence of second-order phase transition [46, 47]. If the Davies point appears then the relationship between QNMs and phase transition still exists [33].

The Davies point occurs where the denominator of the heat capacity (33) ceases. This gives $r_+ = 2k$. This confirms that the Davies point occurs where the values of deviation parameter is half of the horizon radius.

V. NULL GEODESICS AND PHOTON SPHERE

Null geodesics are very important to explain the QNMs of a black hole solution [48]. Here, we follow the photon ring/QNM correspondence [49, 50] to calculate QNMs of this black hole solution in the eikonal limit. To compute the geodesics in spacetime, we first focus on the motion of photons in the black hole solution (16). The Lagrangian for a photon motion limited to equatorial plane ($\theta = \pi/2$) can be expressed as

$$\mathcal{L} = -g_{tt}\dot{t}^2 + g_{rr}\dot{r}^2 + g_{\theta\theta}\dot{\theta}^2 + g_{\phi\phi}\dot{\phi}^2, \quad (34)$$

and the corresponding Hamiltonian is written as

$$\mathcal{H} = p_t\dot{t} + p_r\dot{r} + p_\phi\dot{\phi} - \mathcal{L} \quad (35)$$

where over-dot refers to the derivative with respect to an affine parameter. The generalized momenta are given by

$$p_t = \frac{\partial \mathcal{H}}{\partial \dot{t}} \equiv E = \text{constant}, \quad (36)$$

$$p_\phi = \frac{\partial \mathcal{H}}{\partial \dot{\phi}} \equiv -J = \text{constant}, \quad (37)$$

$$p_r = \frac{\partial \mathcal{H}}{\partial \dot{r}} = g_{rr}\dot{r} \quad (38)$$

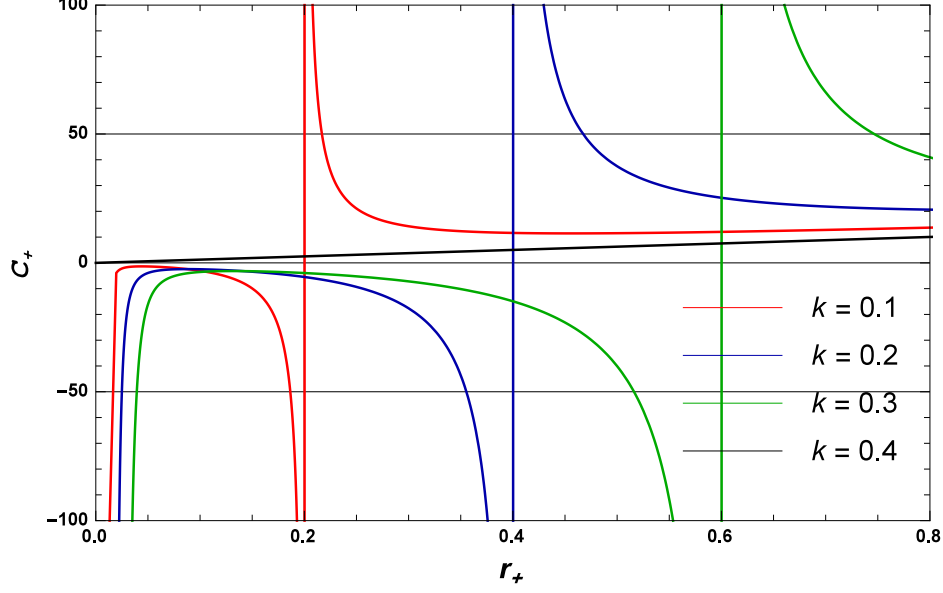


FIG. 2. The plot of specific heat versus horizon radius r_+ for different value of deviation parameter k .

The equation of motion associated with the photon can be calculated using the Hamiltonian formalism, which can be derived as follow

$$\dot{t} = \frac{\partial \mathcal{H}}{\partial p_t} = -\frac{p_t}{g_{tt}}, \quad \dot{\phi} = \frac{\partial \mathcal{H}}{\partial p_\phi} = \frac{p_\phi}{r^2}, \quad \text{and} \quad \dot{r} = \frac{\partial \mathcal{H}}{\partial p_r} = -\frac{p_r}{g_{rr}}. \quad (39)$$

The Hamiltonian is independent of time (t) and azimuthal coordinate (ϕ). The null geodesics equation is given by

$$\dot{r}^2 + V_{eff}(r) = 0, \quad \text{with} \quad V_{eff} = f(r) \left(\frac{J^2}{r^2} - \frac{E^2}{f(r)} \right). \quad (40)$$

For circular null geodesic which describes the radius of the photon sphere, the effective potential must follow the conditions:

$$V_{eff} = \frac{\partial V_{eff}}{\partial r} = 0. \quad (41)$$

The equation of the photon radius (r_p) is calculated as

$$\frac{2(kM - r_p(3M - (1-a)e^{k/r_p}))}{r_p^2(2M - (1-a)e^{k/r_p})} = 0. \quad (42)$$

This equation can not be solved analytically, so we solve it numerically.

We can determine the angular radius of the black hole shadow by setting r to r_p (circular orbit of the photon) in Eq. (41). The shadow radius for this black hole is calculated by

$$r_s = \sqrt{\alpha^2 + \beta^2} = \frac{L_p}{E} = \frac{r}{\sqrt{f(r)}}|_{r=r_p}. \quad (43)$$

Substituting the value of $f(r)$ from Eq. (16) into Eq. (43), then we plug the numerical value of r_p in the obtained equation and the numerical results are presented in TABLE II and TABLE III. It is noticed from the TABLES that the photon radius increases with the deviation parameter and decreases with the CS parameter.

The shadow of the black hole can be visualized with the help of celestial coordinates α and β [51–54]. For the obtained black hole solution the α and β are given by

$$\alpha = \lim_{r \rightarrow \infty} \left(\frac{rp^\phi}{p^t} \right), \quad \text{and} \quad \beta = \lim_{r \rightarrow \infty} \left(\frac{rp^\theta}{p^t} \right). \quad (44)$$

k	r_p				r_s			
	$a = 0.1$	$a = 0.2$	$a = 0.3$	$a = 0.4$	$a = 0.1$	$a = 0.2$	$a = 0.3$	$a = 0.4$
0.0	3.333	3.751	4.285	5.001	0.544	0.516	0.482	0.447
0.1	3.195	3.612	4.148	4.863	0.541	0.511	0.478	0.443
0.2	3.047	3.466	4.004	4.720	0.534	0.505	0.474	0.440
0.3	2.886	3.309	3.851	4.570	0.529	0.497	0.468	0.436
0.4	2.710	3.139	3.687	4.412	0.513	0.480	0.461	0.431
0.5	2.512	2.953	3.511	4.244	0.497	0.477	0.453	0.425
0.6	2.283	2.745	3.318	4.065	0.476	0.463	0.443	0.418
0.7	1.999	2.505	3.105	3.872	0.441	0.440	0.431	0.410

TABLE II. The numerical values of photon radius corresponding to the deviation parameter (k) with fixed CS parameter (a).

a	r_p				r_s			
	$k = 0.1$	$k = 0.2$	$k = 0.3$	$k = 0.4$	$k = 0.1$	$k = 0.2$	$k = 0.3$	$k = 0.4$
0.0	2.8615	2.711	2.587	2.453	0.570	0.560	0.556	0.553
0.1	3.1954	2.041	2.926	2.790	0.541	0.532	0.530	0.528
0.2	3.6126	3.460	3.348	3.220	0.511	0.505	0.502	0.501
0.3	4.1488	4.004	3.889	3.764	0.478	0.474	0.472	0.471
0.4	4.8636	4.720	4.619	4.490	0.444	0.440	0.439	0.438
0.5	5.8641	5.721	5.612	5.490	0.405	0.402	0.402	0.401
0.6	7.3647	7.225	7.117	7.005	0.363	0.361	0.361	0.361
0.7	9.8652	9.727	9.621	9.513	0.315	0.313	0.313	0.313

TABLE III. The numerical values of photon radius corresponding to the CS parameter (a) with fixed deviation parameter (k).

The shadow of the obtained solution for different values of CS parameter (a) and the different values of deviation parameter (k) is depicted in Fig. 3. From the figure we see that the size of the shadow decreases with the increasing CS parameter and deviation parameter (as evident from TABLE II and TABLE III also). As we know the black hole in the limit $r \gg k$, the given black hole corresponds to the Reissner-Nordström black hole with CS parameter. So, we can easily comment that the shadow of the resulting black hole with large horizon radius and small value of k will only match to the shadow of the Reissner-Nordström black hole. However, as the value of deviation parameter will increase the shadow radius of the given black hole will get smaller comparative to the Reissner-Nordström black hole case.

VI. CONNECTION BETWEEN SHADOW RADIUS AND QNMS

The QNMs encode the details about the stability of the black holes under small perturbation and these are described by the $\omega = \omega_R + i\omega_I$. The signature of the ω_I characterizes the stability of the black hole. For instance, $\omega_I > 0$ corresponds to stable modes of black holes and the rest corresponds to unstable modes. The real part and imaginary part of the QNMs in the eikonal limit are associated with the angular velocity and the Lyapunov exponent of (unstable) circular null geodesics, respectively [32, 55]. Such a connection also occurs for the QNMs and gravitational lensing [56]. The real part of QNMs in the eikonal limit is associated with the radius of the black hole shadow [57, 58]. Such connections had already been explored to various black holes [59–61]. The QNMs frequency ω can be estimated through photon sphere as

$$\omega = l\Omega - i \left(n + \frac{1}{2} \right) |\Lambda|, \quad (45)$$

where n is the overtone number and l is the angular quantum number. Here, the angular velocity (Ω) and the Lyapunov exponent (Λ) of the photon sphere are given, respectively, by

$$\Omega = \frac{\sqrt{f(r_p)}}{r_p} = \frac{1}{L_p}, \quad (46)$$

$$\Lambda = \frac{\sqrt{f(r_p)(2fr_p - r_p^2 f''(r_p))}}{\sqrt{2}r_p}. \quad (47)$$

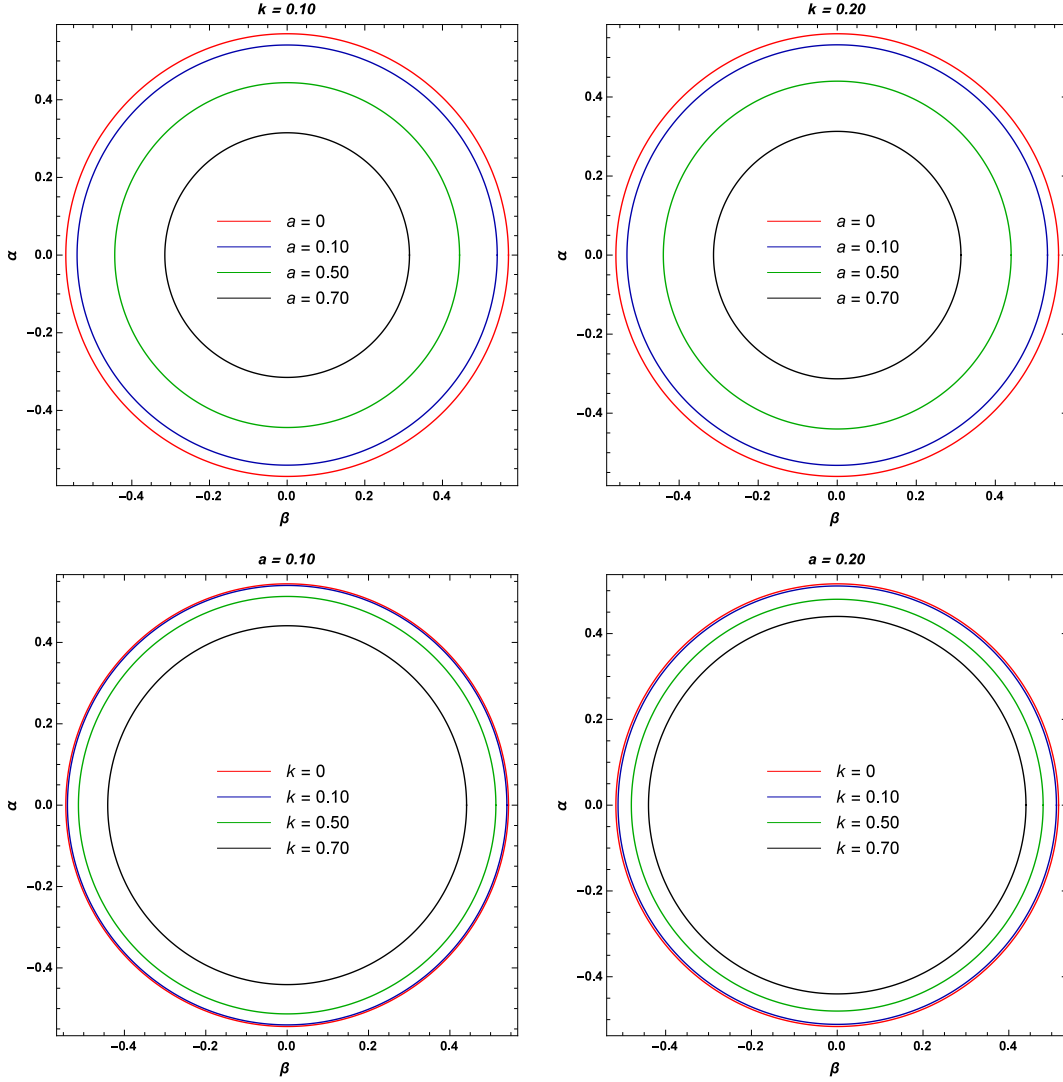


FIG. 3. The plot of black hole shadow corresponding to the CS parameter (a) with fixed deviation parameter (k) (upper panel) and corresponding to the deviation parameter (k) with fixed CS parameter (a) (lower panel).

The QNMs are characterized by complex numbers. The imaginary part of the QNMs tells about the stability of the black hole such that when $Im \omega > 0$ the system is stable and when $Im \omega < 0$ the system is unstable. The real and imaginary parts of the QNMs for the given black hole (16) for different values of deviation parameter (k) and CS parameter (a) are depicted in the figure 4. From the figure, we make the following observations:

1. The upper panel of figure 4 tells that the real (imaginary) part of the QNMs frequency decreases (increases) with increasing the CS parameter. This indicates that the scalar field perturbation in the presence of deviation parameter oscillates faster and decays slower as compared to Reissner-Nordström black hole [62].
2. The lower panel of figure 4 suggests that both the real and imaginary parts of the QNMs frequency increase with the deviation parameter. This means that the scalar field perturbation in the presence of CS parameter oscillates and decays faster as compared to Reissner-Nordström black hole [62].

Here, it is worthwhile to mention that the effects of k and a are opposite to each other. From the right panel of figure 4, we notice that the $Im \omega$ is negative for both k and a . Therefore, the obtained black hole solution is stable.

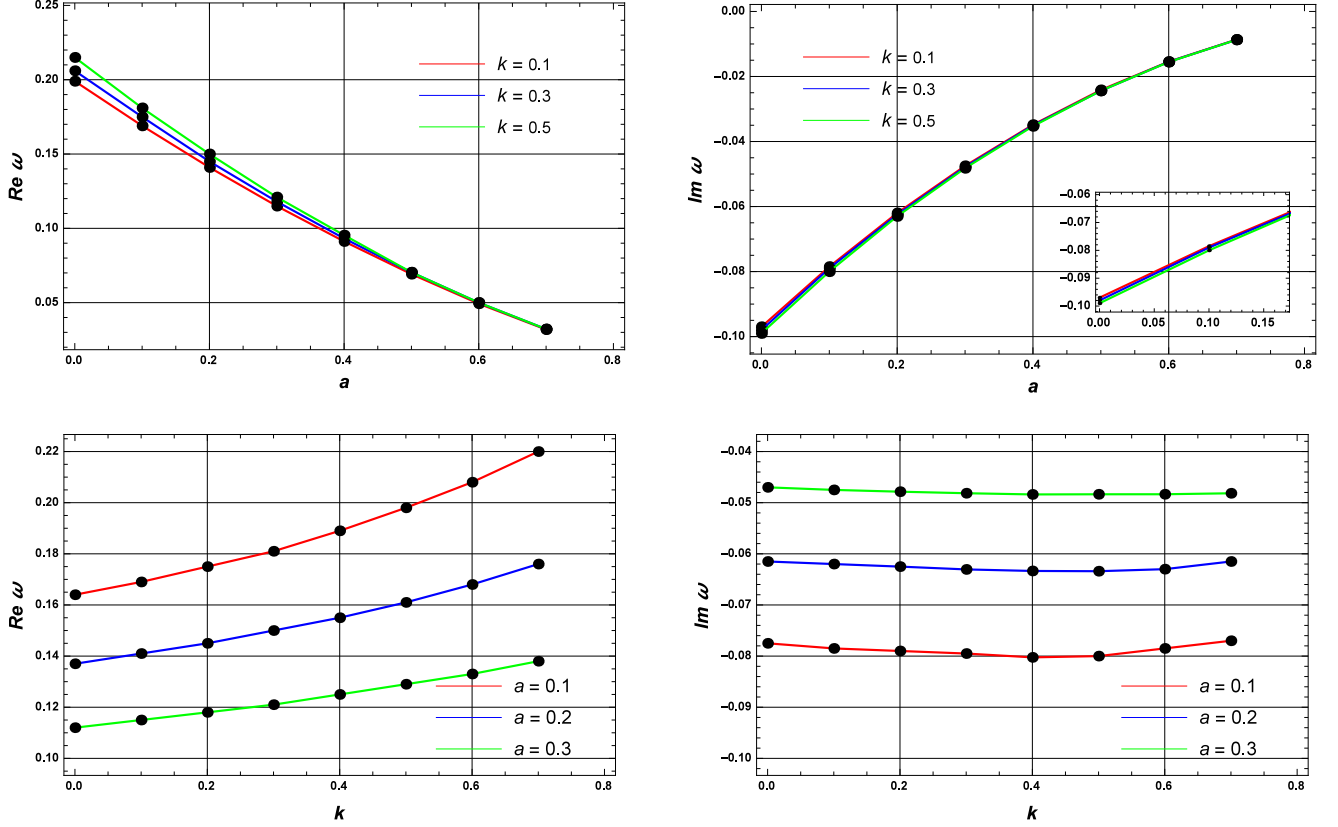


FIG. 4. Upper panel: the real and imaginary part of QNMs with respect to a for different k . Lower panel: the real and imaginary part of QNMs with respect to k for different a .

VII. CONCLUSIONS

The nonlinear electrodynamics as a source of gravity has the possibility to create regular black holes and star (or soliton) like configurations of interest. In this work, we have focused on a gravity model coupled with the nonlinear electrodynamics (which resembles the electrodynamics in the weak field limit) in the presence of a cloud of strings as the source. The dynamics of such the gravity model is described by a suitable action and corresponding equation of motions.

Furthermore, we have discussed the thermodynamics of the black hole solution. The effects of the deviation parameter and CS parameter on the temperature are emphasized. The temperature is a decreasing function of the deviation parameter and CS parameter. Hawking temperature of the black hole is Interestingly, here we have found that instead of the standard first-law of thermodynamics this black hole follows a modified first-law of thermodynamics. From the specific heat, we have found that there is no effect of surrounding CS on the stability of black hole. However, the second-order phase transition occurs at certain point (Davies point), where deviation parameter is half of the value of horizon radius. The existence of Davies point confirms the relationship between QNMs and phase transition. QNMs for this particular black hole solution in the eikonal limit are calculated under the consideration of photon ring/QNM correspondence. The photon radius is obtained numerically. There are many interesting opportunities that can be studied further in future works. For example, it will be interesting to explore the quantum effects on the thermodynamics and stability of the regular black hole solution.

We also study the relation between the shadow radius and QNMs of the solution (16). From the figures 3 and 4, we found that the real and imaginary part of the QNMs decreases and increases with the increasing the CS parameter, respectively. However, and the shadow radius decreases with the increasing the CS parameter. However, the real and imaginary part of QNMs increases with increasing deviation parameter and shadow radius decreases with increasing deviation parameter. The shadow behavior and photon sphere in the presence of black hole parameter k and a are also studied. The numerical results (cf. TABLE II) confirmed that the photon sphere (r_p) and shadow radius (r_s)

are decreasing with the deviation parameter. However, with the CS parameter (cf. TABLE III), the photon radius (r_p) is increasing and shadow radius (r_s) is decreasing.

DATA AVAILABILITY STATEMENT

Data sharing not applicable to this article as no datasets were generated or analysed during the current study.

-
- [1] H. Stephani, D. Kramer, M. MacCallum and C. Hoenselaers, *Exact Solutions of Einstein's Field Equations* (Cambridge University Press, second edition, Cambridge 2002).
 - [2] J. M. Bardeen, in *Proceedings of GR5* (Tbilisi, URSS, 1968).
 - [3] I. G. Dymnikova, *Gen. Relativ. Gravit.* 24, 235 (1992); *Int. J. Mod. Phys. D* 05, 529 (1996); *Int. J. Mod. Phys. D* 12, 1015 (2003).
 - [4] K. A. Bronnikov, *Phys. Rev. D* 63, 044005 (2001).
 - [5] S. A. Hayward, *Phys. Rev. Lett.* 96, 031103 (2006).
 - [6] T. Tangphati, A. Pradhan, A. Banerjee and G. Panotopoulos, *Phys. Dark Univ.* 33 (2021) 100877.
 - [7] J. M. Z. Pretel, A. Banerjee and A. Pradhan, *Eur. Phys. J. C* 82 (2022) 180.
 - [8] T. Tangphati, A. Pradhan, A. Errehymy and A. Banerjee, *Phys. Lett. B* 819 (2021) 136423.
 - [9] R. P. Singh, B. K. Singh, B. R. K. Gupta and S. Sachan, *Can. J. Phys.* 100, 39 (2022).
 - [10] J. C. S. Neves, *Int. J. Mod. Phys. A* 32, 1750112 (2017).
 - [11] M. Born and L. Infeld, *Proc. Roy. Soc. Lond. A* 144, 425 (1934).
 - [12] D. L. Wiltshire, *Phys. Rev. D* 38, 2445 (1988).
 - [13] T. Tamaki and T. Torii, *Phys. Rev. D* 62, 061501 (2000).
 - [14] N. Breton, *Phys. Rev. D* 67, 124004 (2003).
 - [15] S. Fernando and D. Krug, *Gen. Rel. Grav.* 35, 129 (2003).
 - [16] R. G. Cai, D. W. Pang and A. Wang, *Phys. Rev. D* 70, 124034 (2004).
 - [17] A. A. Tseytlin, *Nucl. Phys. B* 276, 391 (1986).
 - [18] L. De Fosse, P. Koerber and A. Sevrin, *Nucl. Phys. B* 603, 413 (2001).
 - [19] P. S. Letelier, *Phys. Rev. D* 20, 1294 (1979).
 - [20] P. S. Letelier, *Il Nuovo Cim. B* 63, 519 (1981).
 - [21] P. S. Letelier, *Phys. Rev. D* 28, 2414 (1983).
 - [22] A. Ganguly, S. G. Ghosh and S. D. Maharaj, *Phys. Rev. D* 90, 064037 (2014).
 - [23] K. A. Bronnikov, S. W. Kim and M. V. Skvortsova, *Class. Quant. Grav.* 33, 195006 (2016).
 - [24] D. Barbosa and V. B. Bezerra, *Gen. Rel. Grav.* 48, 149 (2016).
 - [25] E. Herscovitch and M. G. Richarte, *Phys. Lett. B* 689, 192 (2010).
 - [26] S. G. Ghosh and S. D. Maharaj, *Phys. Rev. D* 89, 084027 (2014).
 - [27] S. H. Mazharimousavi and M. Halilsoy, *Eur. Phys. J. C* 76, 95 (2016).
 - [28] J. L. Synge, *Relativity: The General Theory*, (North Holland, Amsterdam, 1966), p. 175.
 - [29] M. Barriola and A. Vilenkin, *Phys. Rev. Lett.* 63, 341 (1989).
 - [30] S. Chandrasekhar and S. Detweiler, *Proc. R. Soc. Lond. A* 344, 441 (1975).
 - [31] J. Jing and Q. Pan, *Phys. Lett. B* 660, 13 (2008).
 - [32] V. Cardoso, A. S. Miranda, E. Berti, H. Witek and V.T. Zanchin, *Phys. Rev. D* 79, 064016 (2009).
 - [33] K. Jafarzade, M. Kord Zangeneh and F. S. N. Lobo, *JCAP* 04 (2021) 008.
 - [34] S. Mandal, S. Upadhyay, Y. Myrzakulov and G. Yergaliyeva, *arXiv:2207.10085*.
 - [35] S. G. Ghosh, U. Papnoi, and S. D. Maharaj, *Phys. Rev. D* 90, 044068 (2014).
 - [36] S. G. Ghosh, D. V. Singh and S. D. Maharaj, *Phys. Rev. D* 97 (2018) 104050.
 - [37] A. Kumar, D. V. Singh and S.G. Ghosh, *Eur. Phys. Journal C* 79 275 (2019).
 - [38] Md. Sabir Ali and S. G. Ghosh, *Phys. Rev. D* 98, 084025 (2018).
 - [39] D. V. Singh and N. K. Singh, *Annals Phys.* 383, 600 (2017).
 - [40] P. Chaturvedi, N. K. Singh and D. V. Singh, *Int. J. Mod. Phys. D* 26, 1750082 (2017).
 - [41] R. V. Maluf and J. C. S. Neves, *Phys. Rev. D* 97, 104015 (2018).
 - [42] S. G. Ghosh and D. W. Deshkar *Phys. Rev. D* 77, 04750.
 - [43] J. M. Bardeen, B. Carter and S. W. Hawking, *Commun. Math. Phys.* 31 161 (1973).
 - [44] M.-Sen Ma and R. Zhao, *Class. Quantum Grav.* 31 245014 (2014).
 - [45] D. V. Singh, S. G. Ghosh and S. D. Maharaj, *Annals Phys.* 412, 168025 (2020).
 - [46] S. Hawking and D. Page, *Commun. Math. Phys.* 87, 577 (1983).
 - [47] P. Davis, *Proc. R. Soc. A* 353, 499 (1977).
 - [48] S. Chandrasekhar, *The Mathematical Theory of Black Holes*, (Oxford University Press, New York, 1983).

- [49] V. Cardoso, A. S. Miranda, E. Berti, H. Witek, V. T. Zanchin, Phys. Rev. D 79 (2009) 064016.
- [50] N. Breton, L. A. Lopez, Phys. Rev. D 94 (10) (2016) 104008.
- [51] R. Kumar, S. G. Ghosh and A. Wang, Phys. Rev. D 100 (2019) 124024.
- [52] B. P. Singh and S. G. Ghosh, Annals Phys. 395 (2018) 127.
- [53] F. Ahmed, D. V. Singh and S. G. Ghosh, Gen. Rel. Grav. 54 (2022) 21.
- [54] F. Ahmed, D. V. Singh and S. G. Ghosh, arXiv:2008.10241 [gr-qc].
- [55] R. A. Konoplya, Z. Stuchlik Phys. Lett. B **771**, 597 (2017).
- [56] I. Z. Stefanov, Phys. Rev. Lett. 104, 251103 (2010).
- [57] K. Jusufi, Phys. Rev. D 101, 084055 (2020).
- [58] K. Jusufi, Phys. Rev. D 101 124063 (2020).
- [59] Y. Guo and Y. G. Miao, Phys. Rev. D 102 084057 (2020).
- [60] C. Lan, Y. G. Miao and H. Yang, Nucl. Phys. B 971 (2021) 115539.
- [61] S. W. Wei and Y. X. Liu, Chin .Phys. C **44**, 115103 (2020).
- [62] E. W. Leaver, Phys. Rev. D **41** (1990) 2986.